Synthesis and Characterization of Alkoxide-Derived Pt Nanoparticles

H. A. Andreas[†] and V. I. Birss*

Department of Chemistry, University of Calgary, Calgary, Alberta, Canada T2N 1N4

Received: September 15, 2004; In Final Form: December 15, 2004

Identification of the species formed during the in situ reduction of hexachloroplatinic acid by sodium ethoxide, forming a Pt sol, is made. The solution phase is shown to consist of suspended metallic Pt nanoparticles (1−3 nm in diameter), acetaldehyde, and a Pt(II) species, identified by NMR and X-ray adsorption near-edge spectroscopy (XANES) to be $NaPtCl_3(C_2H_4)$, a sodium analogue of Zeise's salt [$KPtCl_3(C_2H_4)$]. The $NaPtCl_3(C_2H_4)$ product exhibits greater stability in both ethanol and air than the conventional Zeise's salt, providing a means of storing the useful Zeise's anion [$PtCl_3(C_2H_4)^-$]. Electrochemistry, X-ray diffraction (XRD), and transmission electron microscopy (TEM) analyses have shown that the precipitate phase formed during the synthesis is composed solely of Pt particles ∼6 nm in diameter and NaCl. Thermal gravimetric analysis/differential scanning calorimetry (TGA/DSC) showed that the color of the precipitate is an accurate gauge of the ratio of Pt to NaCl, with the lightest to darkest precipitates containing from 1% to 40% nanoparticulate Pt by mass, respectively. A comprehensive characterization of both phases formed has allowed us to propose a mechanism for the conversion of hexachloroplatinic acid to Pt nanoparticles.

1. Introduction

Pt nanoparticles are of great interest, due to their high surface area and their catalytic activity toward reactions such as isobutane dehydrogenation[1] and in fuel cell applications, for example, for methanol oxidation[2,3] and oxygen reduction.[4] One common method of Pt nanoparticle formation is the in situ reduction of Pt salts by reducing agents to produce a nanoparticulate powder,[5−9] which can then be supported on a low-cost, high-surface-area support. This method has been previously discussed in the literature, and a number of different reducing agents have been employed, for example, formate,[5] formaldehyde,[5,9] hydrazine,[5,6] borohydride,[10−12] formic acid,[13] sodium citrate,[8,14−16] and sodium thiosulfate.[17] In our previous work with Ir, it was found that the use of similar approaches as employed in sol−gel (SG) syntheses of metal oxides, that is, use of alkoxides, allowed for the preparation of highly porous metallic Ir films[18] (composed of nanoparticles ∼1 nm in diameter), presumably also through an in situ reduction process. However, to our knowledge, the formation of Pt nanoparticles by use of an alkoxide[19] has not yet been explored by others.

The alkoxide route allows the properties of the Pt nanoparticles to be easily optimized, by varying the amount of water employed, the ratio of reactants, the synthesis temperature, and the time;[20] the resulting film thickness and porosity can also be modified by varying the substrate withdrawal rate from the sol, the number of coatings, and the film drying temperature and time.[21] The alkoxide method results in molecularly mixed multielement composites, where species such as Ru,[22] Ir,[23] and W oxide[24] can be added to the Pt sol to enhance its catalytic ability. The specific synthesis used here for Pt sol formation was presented in our previous paper[19] and was shown to produce a precipitate phase and a sol containing suspended metallic Pt nanoparticles ca. 1−3 nm in diameter. However, it was also shown[19] that an unidentified still-oxidized Pt species is also present in the sol phase, lowering the efficiency of Pt nanoparticle formation. X-ray photoelectron spectroscopy (XPS) showed[19] the Pt oxidation state in this product to be +2, and X-ray diffraction (XRD) and quartz crystal microbalance (QCMB) data proved that this material is soluble in water when dried at 22 °C. However, the XRD pattern of this species did not correspond to any known compound; also, the Pt(II) component was shown[25] to undergo a conversion reaction at above 200 °C.

The purpose of this paper is to characterize all of the species formed in the synthesis of several hexachloroplatinic acid (CPA)/sodium ethoxide ($NaOC_2H_5$) formed Pt sols. As well, a mechanism of in situ Pt sol formation via CPA reduction by $NaOC_2H_5$ is proposed, with a goal of enhancing the yield of Pt nanoparticles for use as an electrocatalyst in fuel cell reactions.

2. Experimental Methods

2.1. Pt Sol Synthesis. The synthesis of the Pt sol[19] involves refluxing, under Ar, a mixture of hexachloroplatinic acid (CPA) (ca. 0.12 mol/L Pt) and sodium ethoxide ($NaOC_2H_5$) in various hexachloroplatinic acid (CPA):$NaOC_2H_5$ molar ratios [1:2 (type 1) or 1:5 (type 2)] in 10 mL of absolute ethanol for 2 h, followed by 18 h of stirring under Ar. The precipitate was then filtered under vacuum, and both the sol phase [suspended Pt nanoparticles + soluble Pt(II) species + acetaldehyde] and precipitate were retained separately for examination.

2.2. Electrochemical Methodology. To examine the electrochemistry of the precipitate, a sticky carbon (SC) electrode substrate was used, prepared by mixing carbon black with beeswax in an approximate weight ratio of 1:1. The end of the SC rod electrode was polished until glossy on laser printing paper (Boise, 28 lb). The precipitate was then loaded onto the SC by pressing its end into the loose precipitate, and the loading weight was taken as the difference in weight before and after pressing.

Cyclic voltammetry (CV) and chronoamperometry (CA) were carried out at a Au sputter-coated glass electrode (∼1 cm^2) in

* Corresponding author: phone (403) 220-6432; fax (403) 289-9488; e-mail birss@ucalgary.ca.

[†] Current address: Chemistry Department, University of Ottawa, Ottawa, Ontario.

10.1021/jp045811u CCC: $30.25
Published on Web 02/12/2005

36 mL of 0.5 M H_2SO_4, to which was added either 100 (CV) or 10 μL (CA) of the sol phase. In the CA experiments, the current due to the reduction of any oxidized Pt species remaining in the sol phase was measured at 0.1 V for up to 4 h while the cell solution was stirred with a magnetic stir bar.

The counterelectrode (CE) was a Pt gauze (area ca. 14−22 cm^2) embedded in soft glass tubing. The reference electrode (RE) was a typical reversible hydrogen electrode (RHE) and all potentials are reported vs the RHE. All of the electrochemical measurements were performed in a two-compartment cell, joined by a Luggin capillary, and were carried out at room temperature (22 ± 2 °C). The main compartment was deaerated before and during electrochemical measurements by continuously bubbling N_2 through or over the solution.

Some electrochemical measurements were performed with a PARC EG&G 173 potentiostat and 175 programmer, with the results recorded on an HP 7045B X/Y or an HP 7090A X/Y recorder. Computer-controlled CV was performed with a PARC EG&G 271 potentiostat under Corrware control, with data analysis carried out by use of Corrview software.

2.3. Product Characterization Methods.

X-ray Diffraction. The precipitate and dried films of the Pt sol were examined by XRD. The precipitate sample was suspended in acetone and deposited onto the glass slide, followed by evaporation of the acetone. Thick samples of the dried Pt sol were formed by repeatedly drying, in air, aliquots (ca. 20 μL) of the sol on the slide. Data were obtained by use of a Rigaku Multiflex powder diffractometer (Department of Geology and Geophysics, University of Calgary). The patterns were then compared to the JADE XRD Pattern Processing[25] database.

Transmission Electron Microscopy. TEM analysis of the precipitate was achieved by first suspending it (0.9 mg) in 0.6 mL of ethanol by sonicating for ca. 2 min. An aliquot of the slurry was then deposited on carbon-coated Cu TEM grids with an Eppindorf pipet and dried at 22 °C. The TEM analyses were carried out on a Hitachi H-7000 TEM with a 75 keV accelerating voltage (Health Sciences Centre, University of Calgary).

Thermogravimetric Analysis/Differential Scanning Calorimetry. TGA/DSC was performed on ca. 1 mg of both the precipitate and the dried sol, on a Netzsch (STA 229C Jupiter) instrument. The measurements were performed in alumina pans by heating at 5 °C/min to a maximum temperature of 1400 °C. Both the protective and purge gases were nitrogen, with gas flow rates of 30 and 10 mL/min, respectively.

X-ray Absorption Near-Edge Spectroscopy. A piece of Al foil was coated with the Pt sol at a withdrawal rate of 120 cm/min and dried in air at 22 °C. XANES was run on the 20-BM (PNC-CAT) line at the Advanced Photon Source (APS) at the Argonne National Laboratory in Argonne, IL, in both fluorescence and transmission modes, between energies of 11.35 and 12.55 keV. The L-III edge was referenced to a Pt foil, set to the standard 11.564 keV. Metallic Pt, $PtCl_2$, and $PtCl_4$ were used as standards for the determination of Pt oxidation states.

Inductively Coupled Plasma Atomic Emission Spectroscopy. Three 0.100 mL aliquots of the sol were mixed with 5 mL of aqua regia to dissolve the Pt suspended in the sol phase and then diluted 10000× with triply distilled water. These solutions were then analyzed by ICPAES, by use of the 265.9 and 214.4 nm lines.

Multinuclear Magnetic Resonance Spectroscopy. NMR analysis of the Pt sol phase involved examining the ^1H, ^{13}C, and ^{195}Pt nuclei on a Brueker 300 MHz NMR spectrometer. The ^1H NMR spectrum was obtained with $CDCl_3$ to lock in the signal and was recorded between −10 and +15 ppm at a frequency of 300 MHz. The ^{195}Pt NMR spectrum was referenced to a K_2PtCl_4/D_2O solution (set to −1628 ppm[1]) [the shift of this reference was set to this value to be in accordance with the measured value for K_2PtCl_4/D_2O, as per Carr et al.[26]] and was recorded from 1000 to −5000 ppm at a frequency of 54 MHz. The ^{195}Pt and ^1H NMR spectra were also run coupled and decoupled from each other. ^{13}C NMR was executed at a frequency of 300 MHz, and both a regular and distortionless enhancement by polarization transfer (DEPT) ^{13}C analysis was recorded in a spectrum window of −5 to 185 ppm.

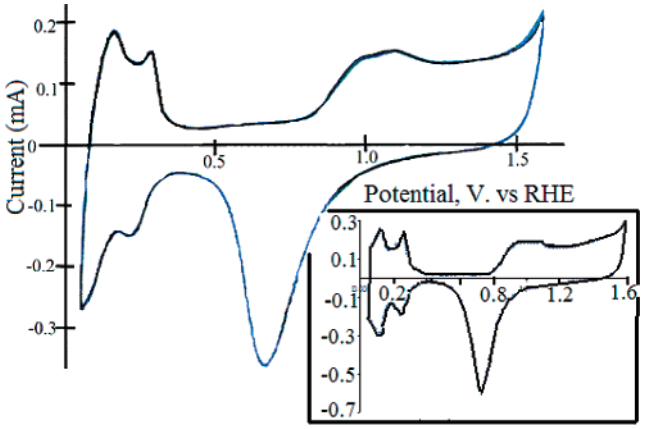

Figure 1. CV (100 mV/s) of type 2 precipitate (2.4 mg pressed on SC electrode) in deaerated 0.5 M H_2SO_4. Inset: CV of bulk Pt foil under the same conditions.

Similarly, the ^1H NMR of the head gas collected during the reflux step during sol formation was examined. To sample the head gas, 15 3-mL aliquots of the head gas were removed from above the sol phase during reflux. This gas was transferred to sealed vacuum vials and placed in an ice bath to condense. The ^1H NMR spectrum, between 0 and 13 ppm, was collected on a 200 MHz Oxford Spectrospin NMR, with $CDCl_3$ to lock the signal.

3. Results and Discussion

3.1. General Observations during Pt Sol Synthesis. Upon mixing of hexachloroplatinic acid (CPA) and $NaOC_2H_5$ in various ratios in ethanol during type 1 and 2 Pt sol synthesis, an orange/yellow solution resulted, which maintained its color throughout the reflux step. When filtered, two phases were obtained, a white/gray (type 1) or dark/black (type 2) precipitate and an orange (type 1) or light yellow (type 2) supernatant (the sol phase). The formation of two phases is also seen during Ir nanoparticle formation,[18] where the majority of the Ir remains suspended as nanoparticles in the black sol phase.

3.2. Characterization of Precipitate Phase Formed during Pt Sol Synthesis. Considering the reactants employed in the synthesis, both metallic Pt and NaCl, among other species, can be expected to form (eq 1). As neither of these is appreciably soluble in ethanol, it was anticipated that both would be found, to varying extents, in the precipitate phase.

$$H_2PtCl_6 + NaOC_2H_5 \rightarrow Pt(0) + NaCl + \text{acetaldehyde} + ? \quad (1)$$

3.2.1. Electrochemistry of Precipitate Phase. Figure 1 shows the CV response of a sticky carbon (SC) electrode, loaded with the black type 2 precipitate, in 0.5 M H_2SO_4. (Due to its high solubility in this solution, a similar study with the white/gray type 1 precipitate was impossible.) Initially, a resistive CV was seen, while with further cycling, a clean, steady-state

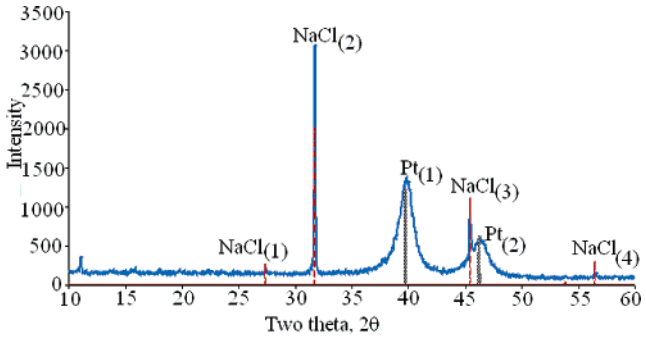

Figure 2. XRD pattern of a type 2 precipitate formed during Pt sol synthesis and the reference Pt [$Pt_{(1-2)}$] and NaCl [$NaCl_{(1-4)}$] peak positions.

response, typical of Pt, is observed. The Pt oxidation plateau (1.0−1.6 V) and reduction peak (centered at 0.7 V) are both evident (cf. with bulk Pt foil CV in Figure 1 inset). As well, the hydrogen underpotential deposition (H upd) peaks of Pt (0.05−0.4 V) are seen but are less well defined than those on bulk Pt, likely due to the resistance associated with the SC. While these results demonstrate conclusively that Pt is a key component of the precipitate, this approach does not allow for particle size determination. It also does not allow a quantitative analysis of the precipitate phase, as the true loading is unknown due to some dissolution of the precipitate upon initial immersion into the solution.

3.2.2. Pt Particle Size in Precipitate Phase. Figure 2 shows the X-ray diffraction (XRD) pattern of the precipitate phase of a type 2 sol. Two phases are clearly present, NaCl [the sharp peaks at 2θ of ~27.4, 31.7, 45.5, and 56.5 (peaks $NaCl_{(1-4)}$)], and metallic Pt [broad peaks at 2θ of 39.8 and 46.3 (peaks $Pt_{(1-2)}$)]. By use of the Scherrer equation,[27] the average Pt particle size in the precipitate was found to be 6 ± 1 nm. As seen by the narrowness of the $NaCl_{(1-4)}$ peaks, limited only by instrumental broadening, the NaCl crystallite size is likely significantly greater than 100 nm.[25]

To confirm the Pt particle size determined by XRD analysis, a slurry of the type 2 precipitate was applied to a carbon-coated Cu TEM grid and the solvent was evaporated. A TEM image (Figure 3) and its related histogram show that the average Pt particle size (based on 30 particles) is 6 ± 2 nm. Neither the large particle in the upper left, nor the very large ovoid grain in the bottom center of the image, was included in this calculation, as the former is an accumulation of the small Pt particles and the latter an agglomeration of the carbon coating the grid.

The size of the Pt particles in the precipitate phase is 2−3 times the average size of the suspended Pt nanoparticles in the sol phase, as measured by TEM.[19] It is possible that their larger size is responsible for their precipitation and/or that they have been coprecipitated with the insoluble NaCl. This latter explanation is supported by our previously shown SEM images of the Pt sol formed film,[19] which show small particles of metallic Pt trapped in or around the NaCl crystals. This is also supported by the results of our work on the optimization of the sol, which shows that, in the absence of NaCl formation, no metallic Pt precipitates from these sols.[20]

3.2.3. Determination of Pt Content of Precipitate Phase. Thermogravimetric analysis (TGA)/differential scanning calorimetry (DSC) analyses were run on a type 1 (white/gray) and a type 2 (black) precipitate under N_2, between 22 and 1400 °C, with a 5 °C/min temperature ramp rate. Consistent with the XRD results, the absence of any Pt compounds with melting (m) or

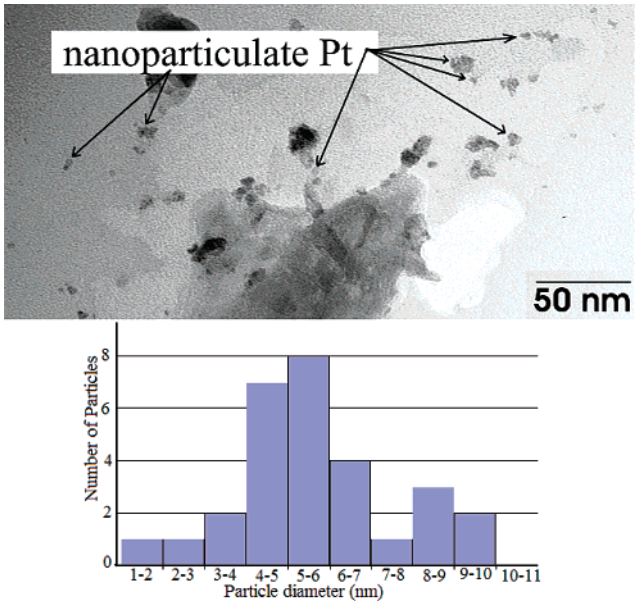

Figure 3. TEM image of Pt particles in a type 2 precipitate supported on a carbon-coated Cu TEM grid and associated histogram of Pt particle size.

decomposition (d) temperatures below 800 °C [i.e., H_2PtCl_6 (m 60 °C), PtO (d 325 °C), $PtCl_4$ (d 327 °C), $PtCl_3$ (d 400−435 °C), PtO_2 (m 450 °C), and $PtCl_2$ (d 581 °C)] is confirmed by Figure 4, which shows no significant mass loss, nor any appreciable enthalpy change, in either sample type at temperatures below 800 °C. At 800 °C, both precipitate samples show a large endothermic enthalpy peak, corresponding to the melting of NaCl (m 801 °C), accompanied by a significant mass loss above 800 °C. This is due to the reaction of the molten NaCl with the alumina sample pans, as confirmed by a similar reaction with a pure NaCl standard, run multiple times under similar conditions (Figure 4c), showing a mass loss of 98.6% ± 0.2% at 801 °C.

By use of the mass loss of a pure NaCl standard, the percentage of NaCl in the sample was determined to be 98% (2% Pt) for the type 1 precipitate, while the black type 2 precipitate was found to contain 61% NaCl (39% Pt), by use of eq 2. These results support the supposition that the color of the precipitate is a direct indicator of its Pt content and also demonstrate that the molar ratio of reducing agent to CPA is a key variable in the yield of the small Pt nanoparticles retained in the sol phase vs the somewhat larger particles found in the precipitate.[20]

$$\frac{\text{100\% NaCl in standard}}{\text{\% mass loss in TGA of standard}} = \frac{\text{\% NaCl in sample}}{\text{\% mass in TGA of sample}} \quad (2)$$

3.3. Characterization of Pt Sol Phase Species. The sol phase has been shown to contain suspended Pt nanoparticles,[19] with sizes in the range of 1−3 nm (Figure 5), and an unknown quantity of an oxidized Pt species, suggested earlier to be in the Pt(II) state by XPS.[19] To verify the presence of the Pt(II) product in these sol phases, CVs of a 0.1 mL aliquot of a type 1 sol, dissolved in 36 mL of 0.5 M H_2SO_4, were collected at a Au sputter-coated glass electrode. Initially, a large cathodic current was observed (Figure 6a), commencing at 0.2 V. This is attributed to the reduction of a Pt(II) species to Pt(0), as seen by the rise of the H upd peaks, characteristic of metallic Pt, and the observation that, with cycling below 0.1 V, the Au

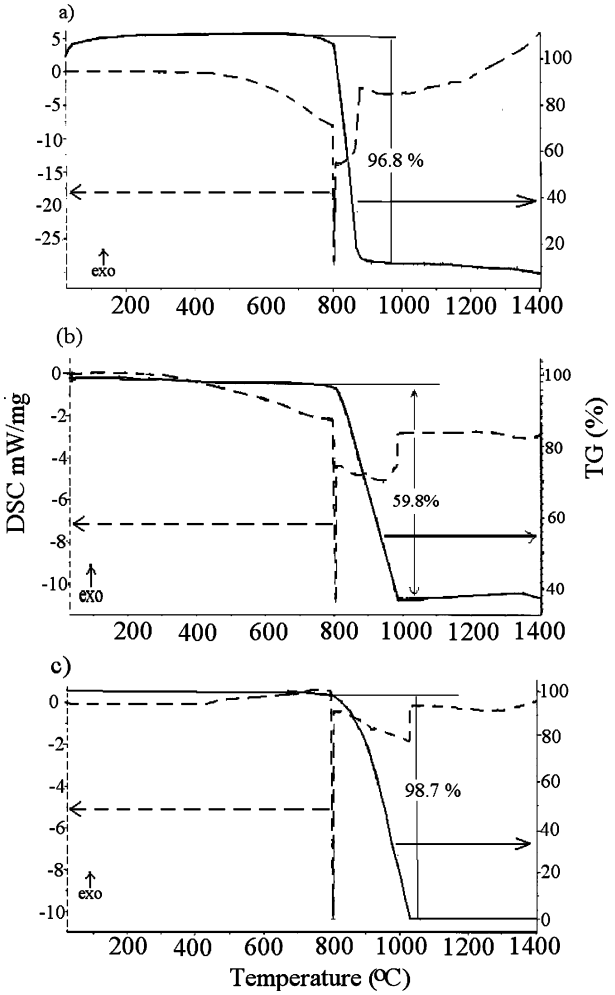

Figure 4. TGA (—) and DSC (---) data, recorded under N_2 at 5 °C/min, of (a) white/gray type 1 precipitate, (b) black type 2 precipitate, and (c) NaCl standard.

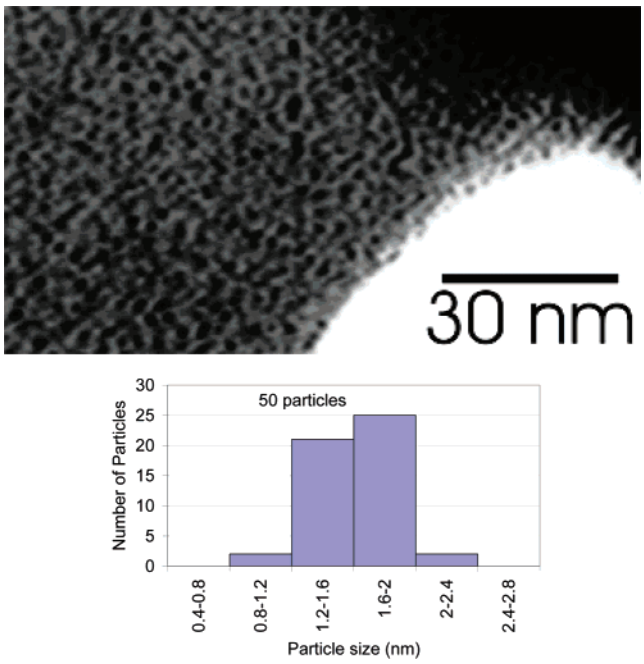

Figure 5. TEM image and related histogram of a type 1 Pt sol, formed on a Cu grid by withdrawal at 24 cm/min and dried at 22 °C for 24 h.

electrode developed the silvery color of Pt. Also, the steady-state CV (Figure 6b) is very similar to that of bulk Pt in a 0.1

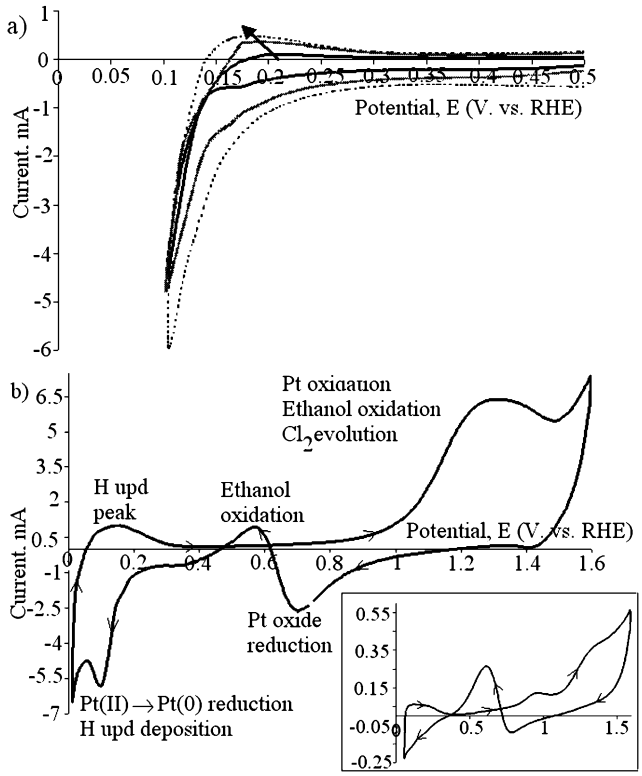

Figure 6. (a) CV scans of a 0.1 mL aliquot of a type 1 Pt sol, in 36 mL of 0.5 M H_2SO_4, run at 100 mV/s on a Au sputter-coated glass electrode. Third (black), fifth (gray), and ninth (dashed) cycles are shown. (b) Steady-state CV response achieved by ca. 3 min of cycling between 0.0 and 1.6 V vs RHE. Inset: CV (100 mV/s) of a bulk Pt foil electrode in 0.1 mL of ethanol in ca. 36 mL of 0.5 M H_2SO_4.

TABLE 1: Binding Energies[a] for Type 1 Pt Sol and Pt Standards of Various Oxidation States

sample	binding energy (keV)
Pt foil	11.5615
$Pt(II)Cl_2$	11.5628
$Pt(IV)Cl_4$	11.5637
Pt sol formed film	11.5623

[a] Recorded at the inflection point of the XANES edge.

mL ethanol + 36 mL 0.5 M H_2SO_4 solution (inset to Figure 6b). The H upd peaks and Pt oxide reduction peak are clearly seen at 0−0.2 V and at 0.7 V, respectively. As well, ethanol oxidation appears to occur over the entire potential window of 0.4−1.6 V, distorting the normal Pt CV. Cl_2 evolution and Au oxide formation/reduction may also be occurring but are not obvious in Figure 6b, as they are obscured by the oxidation of ethanol.

3.3.1. Identification of Pt(II) Product Present in Sol Phase. To identify the soluble form of Pt remaining in the sol phase, X-ray absorption near-edge spectroscopy (XANES) was performed on a type 1 Pt sol formed film (XANES data are not available for type 2 sols), coated on Al foil and dried at 22 °C. To facilitate oxidation state determination under the specific conditions of the beamline, three standards were run for comparison: Pt foil, $PtCl_2$, and $PtCl_4$. Table 1 shows the inflection points of the edge peak for each of these standards and the sample and reveals that the oxidized Pt species has an energy closest to that of the $Pt(II)Cl_2$ standard, indicating that the Pt oxidation state is +2, consistent with the XPS data reported in our previous paper.[19] These results indicate that the Pt(IV) precursor has indeed been reduced but that not all of it has resulted in Pt(0) formation.

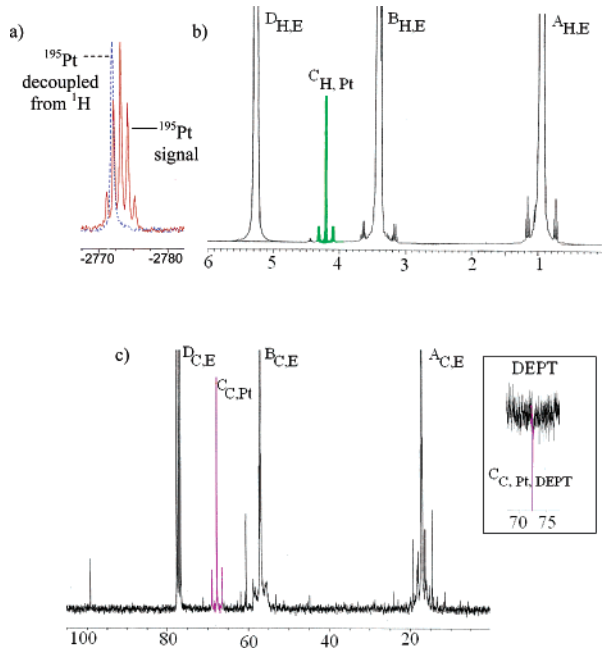

Figure 7. NMR spectra of type 1 Pt sol phase species. (a) ^{1}H-coupled (—) and decoupled (---) ^{195}Pt NMR spectra. (b) ^{1}H NMR spectrum with Pt-coupled proton peak ($C_{H,Pt}$) and ethanol peaks ($A_{H,E}$, $B_{H,E}$, and $D_{H,E}$) (from solvent of sol). (c) ^{13}C NMR spectrum of type A_2 Pt sol, exhibiting Pt coupling in peak $C_{C,Pt}$ and ethanol peaks ($A_{C,E}$, $B_{C,E}$, and $D_{C,E}$). Inset: DEPT of this C NMR spectrum ($C_{C,Pt,DEPT}$).

NMR was then used for the absolute identification of the Pt(II) species present in the sol phase. The one ^{195}Pt peak in evidence in the window of −5000 to 1000 Hz (solid line Figure 7a) is split into a quintet (−2771.2, −2772.2, −2773.2, −2774.3, and −2775.5 ppm in ratios of 1:4:6:4:1), indicating that the Pt(II) ion is coupled with four spin $^{1}/_{2}$ species in identical environments. The coupling constant measured for this peak (64 Hz) was identical to that found for a singlet at 4.20 ppm (with satellites at 4.31 and 4.09) seen in the ^{1}H NMR (peak $C_{H,Pt}$ in Figure 7b), establishing that the Pt was coupled with four equivalent protons. As well, the integration of the satellite area of the ^{1}H signal comprises 34% of the total signal, agreeing with the 34% natural abundance of spin $^{1}/_{2}$ Pt, supporting this identification. This was further confirmed when the ^{195}Pt NMR signal was decoupled from ^{1}H, whereupon the quintuplet then became a singlet (dashed line in Figure 7a). Similarly, when ^{1}H NMR spectroscopy decoupled from ^{195}Pt NMR was run, the satellites of the peak were no longer seen. As Pt would not readily bear a negative charge and as the H is not a hydride, the protons must be coupling to Pt through another atom.

To determine whether the protons were bonded to the Pt through a C species, the ^{13}C and DEPT analyses were run (Figure 7c). The peak at 67 ppm ($C_{C,Pt}$) in the ^{13}C spectrum is characteristic of C coupled to a spin $^{1}/_{2}$ Pt atom. Again, integration of the satellite peak area yielded 34% of the total area, confirming this supposition. When DEPT was run on the sample, the peak was confirmed as being due to a CH_2 group. This, combined with the ^{1}H NMR results, confirmed that two CH_2 carbons are coupled with Pt in the Pt(II) species in the sol phase.

The only arrangement in which two equivalent CH_2 groups could be bonded only to Pt is in a Pt−ethylene dative bond.[28] This type of bonding is evidenced in species such as Zeise's anion (Figure 8),[29−32] containing a Pt(II) center, which tallies with our XPS[19] and XANES results. When the ^{1}H NMR spectrum of the ionic form of Pt in the sol phase was compared

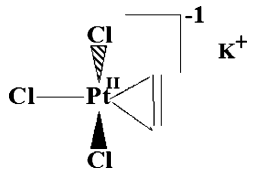

Figure 8. Zeise's salt in potassium ion form.

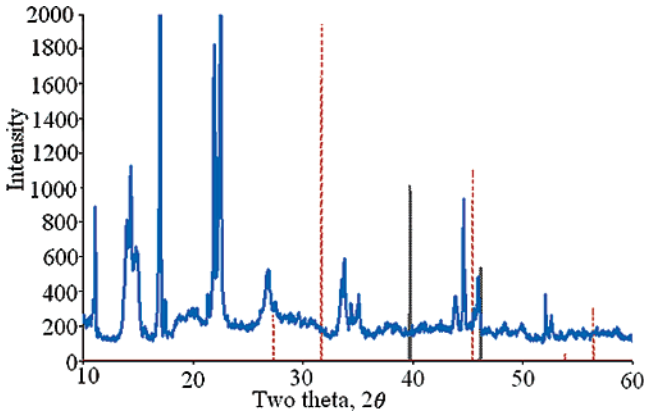

Figure 9. XRD pattern of typical Pt sol (type 1) dried on glass XRD plate, with the lines for the NaCl reference (dashed lines) and metallic Pt (gray lines) also shown.

to that of Zeise's compound, the peak shifts were found to match exactly.[31] However, as will be discussed later, Zeise's anion is commonly found with a K^+ counterion [producing Zeise's salt, $KPtCl_3(C_2H_4)$], whereas the counterion used in the present synthesis is Na^+. Thus, the oxidized species in the Pt sol phase is identified as $PtCl_3(C_2H_4)^-$, and exists as $NaPtCl_3(C_2H_4)$ in the sol formed films. To date, no literature has been found wherein Na^+ was used as the counterion for Zeise's anion.

Literature on Zeise's salt (Figure 8) discusses the fact that it rapidly decomposes in ethanol and in air to produce metallic Pt, and thus, an initially yellow ethanol solution will soon turn black, as will the yellow crystals upon exposure to air.[29] However, our oxidized Pt product is stable in ethanol and in air and both the sol and dried crystals remain unchanged in color for years, indicating that no further reduction is occurring in solution. Thus, by changing the counterion from K^+ to Na^+, we have greatly enhanced the stability of Zeise's anion, in both air and ethanol.

XRD analysis of the sol phase shows (Figure 9) that at least one well-defined crystalline phase, presumably $NaPtCl_3(C_2H_4)$, is present in the dried Pt sol phase. However, a match to the pattern of any known Pt compound in the JADE (release 5.0.12) database or to the theoretical pattern of the conventional Zeise's salt could not be made (an extensive literature search provided no experimental XRD pattern for Zeise's salt, likely due to its instability in air). However, the lack of a direct match is unsurprising, as a simple change of the counterion (Na for K) can result in a substantial change in the XRD pattern.[33] Thus, XRD cannot be used to confirm the identity of our species but is nonetheless valuable as the first XRD pattern of our newly synthesized $NaPtCl_3(C_2H_4)$.

Literature on Zeise's salt indicates[29] that it undergoes thermal decomposition at ~200 °C. Therefore, TGA/DSC analysis of a type 1 Pt sol was carried out. Figure 10 shows an initial small mass loss between 22 and 200 °C, likely due to the evaporation of residual ethanol and possibly water from the powder. The absence of starting material after the reaction is confirmed by the lack of an endothermic peak in the DSC at 60 °C (the melting point of H_2PtCl_6). The large mass loss in the region

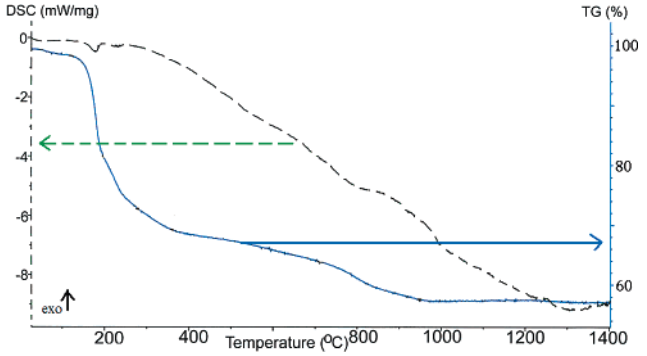

Figure 10. TGA/DSC results recorded for the dried type 1 Pt sol, run under N_2 atmosphere at 5 °C/min.

near 200 °C is attributable to further removal of organics and to the thermal conversion of $NaPtCl_3(C_2H_4)$ to another Pt(II) crystalline species and metallic Pt,[19] as confirmed by XPS (results not shown). Above 200 °C, there are several other mass losses seen, none of which corresponds to the melting or decomposition of any known Pt compounds. Due to the high melting point of metallic Pt (1769 °C[34]), the Pt nanoparticles are not detectable by TGA/DSC, although ca. 57% of the mass remains at 1400 °C, likely attributable to metallic Pt.

When the ^1H NMR spectrum of the Pt sol was examined more closely, acetaldehyde was also found to be present (as expected from eq 1), although in low quantities, likely as it was lost to the atmosphere when the refluxing vessel was opened to atmosphere at the completion of the synthesis. This was confirmed in an experiment in which the head gas above an actively refluxing solution was sampled, cooled, and then examined by ^1H NMR. Figure 11 shows that the acetaldehyde peaks are now indeed much more prominent (peaks aa_q and aa_t in inset).

3.3.2. Quantification of Zeise's Anion (in Na Form) in Sol Phase. To quantify the amount of $NaPtCl_3(C_2H_4)$ in the type 1 sol phase, a 10 μL aliquot was added to 36 mL of 0.5 M H_2SO_4 in the electrochemical cell and the current at 0.1 V (the reduction potential of the oxidized Pt species) was measured for up to 4 h, while the cell solution was stirred with a magnetic stir bar. Pt deposition was visually confirmed by the formation of a gray/black film on the Au electrode. After ca. 3 h, the electrode was lowered further into the solution and the reduction was continued for another hour. The absence of further Pt deposition on the newly submerged Au electrode confirmed the completion of the reduction.

The total charge passed was then multiplied by $^2/_3$, assuming that, for every three electrons passed, two were used to reduce Pt(II) to Pt(0) and one was used for the H upd reaction on the newly formed Pt atoms. Then, the charge due to Pt reduction (q_{Pt}) was converted to the number of moles of Pt (n_{Pt}). This experiment showed that ca. 25% of the original $PtCl_6^{2-}$ is still in the Pt(II) form and has not been reduced to Pt(0).

To determine what fraction of the metallic Pt metal resides in the sol phase as suspended nanoparticles vs in the precipitate, inductively coupled plasma atomic emission spectroscopy (ICPAES) was performed on the type 1 sol. To ensure complete dissolution of the Pt nanoparticles, 100 μL aliquots of the sol were dissolved in aqua regia for 48 h, diluted 10 000-fold in distilled water, and then analyzed. It was found that the total concentration of Pt in the original, undiluted type 1 sol is 29.0 $\pm$ 0.8 ppt (0.119 $\pm$ 0.003 M, with the density of absolute ethanol of 0.80 g/mL), and with the volume of the sol after refluxing (8.5 mL), this is equivalent to a total mass of Pt of 0.20 g. This is 1.6% less than expected if all of the Pt added as the starting material (H_2PtCl_6) remained in the sol (this 1.6% difference has been determined to be significant, rather than due to any error, by a statistical error analysis). These data indicate that, in the formation of this particular sol, the precipitate contained 1.6% of the original Pt, which is borne out by its white color and corresponds exactly to the amount of Pt found in it by TGA/DSC. By combining the electrochemical and ICPAES data, the percent conversion of the Pt(IV) precursor to metallic Pt in the sol was calculated. For the type 1 sol, ~75% of the total Pt content of the sol [(1.10 $\pm$ 0.07) $\times$ 10^{-6} moles] exists as suspended metallic Pt nanoparticles, and 25% [(3.9 $\pm$ 0.7) $\times$ 10^{-7} mol] remains as $PtCl_3(C_2H_4)^-$.

3.4. Mechanism of Formation of Metallic Pt with Ethoxide as Reducing Agent. The first step in the reduction mechanism is suggested to be the exchange of a chloride ion from H_2PtCl_6

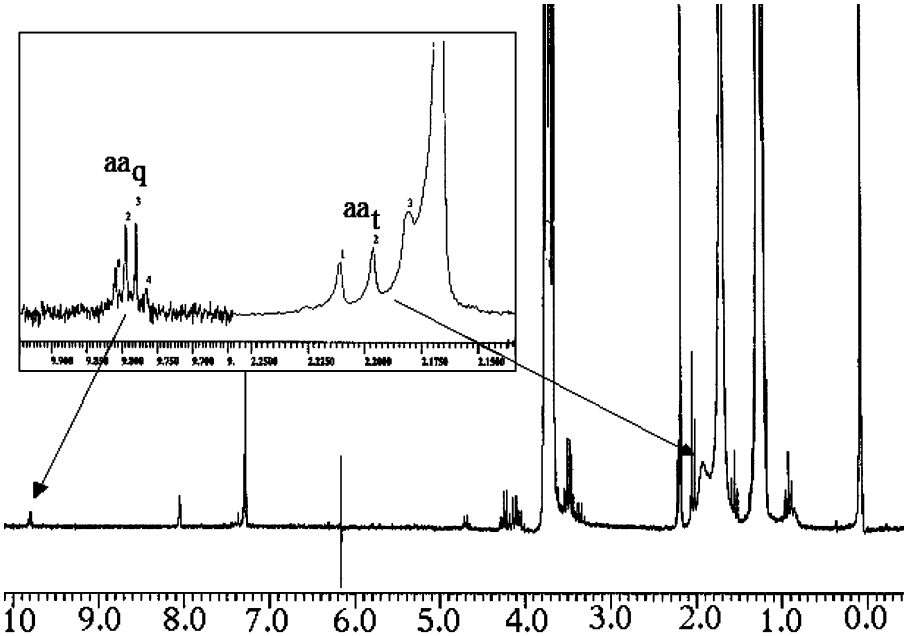

Figure 11. NMR evidence of acetaldehyde in head gas collected above type 1 Pt sol during the reflux step. The two peaks for acetaldehyde are shown by aaq and aat, and the coupling constant for these peaks is 2.9 ppm.

with an ethoxide group from $NaOC_2H_5$, yielding an unstable $PtCl_5(OC_2H_5)^{2-}$ intermediate and NaCl in a metathesis reaction (eq 3). Evidence for the high yield of NaCl in the precipitate has been presented by XRD and TGA/DSC data, consistent with the low solubility of NaCl in ethanol. As well, evidence for a small amount of NaCl in the sol phase is shown by SEM and XPS.[19] The $PtCl_5(OC_2H_5)^{2-}$ intermediate is likely too unstable to be identified by any of the techniques described above. However, its further reaction to acetaldehyde (eq 4) was seen by NMR in both the Pt sol and the head gas, as $PtCl_5(OC_2H_5)^{2-}$ is suggested to undergo β-hydride elimination, producing acetaldehyde and likely $PtCl_5H^{2-}$ (eq 4). This species then undergoes a rapid reductive elimination step (eq 5), producing HCl and $PtCl_4^{2-}$. The Pt(IV) center has now been reduced to Pt(II), and the process begins again, eventually reducing Pt(II) to Pt(0) (eqs 6−8), as seen in the precipitate by CV and XRD and in the sol by CV, SEM, and XPS:[19]

$$[Pt(IV)Cl_6]^{2-} + Na^+ + OC_2H_5^- \rightarrow [Pt(IV)Cl_5(OC_2H_5)]^{2-} + NaCl \quad (3)$$

$$[Pt(IV)Cl_5(OC_2H_5)]^{2-} \rightarrow [Pt(IV)Cl_5H]^{2-} + CH_3COH \quad (4)$$

$$[Pt(IV)Cl_5H]^{2-} \rightarrow [Pt(II)Cl_4]^{2-} + HCl \quad (5)$$

$$[Pt(II)Cl_4]^{2-} + Na^+ + OC_2H_5^- \rightarrow [Pt(II)Cl_3(OC_2H_5)]^{2-} + NaCl \quad (6)$$

$$[Pt(II)Cl_3(OC_2H_5)]^{2-} \rightarrow [Pt(II)Cl_3H]^{2-} + CH_3COH \quad (7)$$

$$[Pt(II)Cl_3H]^{2-} \rightarrow Pt(0) + HCl + 2Cl^- \quad (8)$$

In a parallel process, we have also shown that some $PtCl_3(C_2H_4)^-$ is formed, likely by reaction of the $PtCl_6^{2-}$ anion, arising from the starting material, with the ethanol solvent under reflux conditions. This is analogous to the well-known and characterized reaction of Anderson,[35] wherein potassium hexachloroplatinate (K_2PtCl_6) is refluxed in ethanol, resulting in Zeise's salt [$KPtCl_3(C_2H_4)$].

It is possible that the $PtCl_3(C_2H_4)^-$ product stabilizes the suspended Pt nanoparticles, similar to what has been found with other ionic stabilizers.[8,14,36−39] This is supported by the TEM and TGA/DSC findings, which showed that in the type 2 sol synthesis, a large percentage of the metallic Pt formed is found in the precipitate, rather than in the sol. Conversely, with a type 1 sol, almost the entire metallic Pt content is found to consist of Pt nanoparticles suspended in the sol, and very little is in the precipitate. This is likely due to a deficit of the stabilizing $PtCl_3(C_2H_4)^-$ anion in the type 2 sol, as it has been more fully reduced by the excess reducing agent present. Thus, although the presence of the $PtCl_3(C_2H_4)^-$ product signals that the CPA starting material has been incompletely reduced to metallic Pt, its presence may be beneficial in stabilizing uniformly small suspended Pt nanoparticles. Given that the goals of electrocatalyst formation include the synthesis of stable, high surface area particles, with an efficient usage of the catalyst metal, these very small Pt nanoparticles are ideal. Indeed, it will be shown[20] that the synthesis involved in making type 1 sols yields optimum results (high yield of high-surface-area Pt) when the Pt nanoparticles are deposited on an electrode substrate directly from the sol phase.

Summary

The formation of Pt nanoparticles by the reaction of hexachloroplatinic acid (CPA) with sodium ethoxide, in ethanol, has been investigated in detail. Two phases result: a precipitate, which ranges from white to black in color, depending on the CPA to ethoxide ratio, and a yellow or orange-colored solution phase. From the cyclic voltammetry, X-ray diffraction (XRD), and thermal gravimetric analysis/differential scanning calorimetry (TGA/DSC) results, it has been shown that the precipitate is composed entirely of small Pt particles (average diameter of 6 nm) and NaCl. The TGA/DSC data showed that the darker precipitates contain a higher percentage of metallic Pt than do the lighter-colored ones. As well, in the optimized sol synthesis (type 1, with a 2:1 sodium ethoxide to CPA ratio), only 1% of the Pt is lost to the precipitate.

Electrochemical and inductively coupled plasma spectroscopic results showed that, of the Pt species retained in the sol, ∼75% was in the form of Pt nanoparticles (1−3 nm diameter) and ∼25% existed in a Pt(II) form (seen by X-ray photoelectron spectroscopy and X-ray absorption near-edge spectroscopy). The Pt(II) species was identified, by NMR spectroscopy, as being a Na^+ analogue of Zeise's salt [$KPtCl_3(C_2H_4)$], which exhibited a greater stability in both ethanol and air than the typical K^+ form of Zeise's salt. The $NaPtCl_3(C_2H_4)$ species, which arises from a side reaction of H_2PtCl_6 and ethanol, rather than as an intermediate formed during the in situ Pt(IV) reduction reaction, may serve as a stabilizer for the Pt nanoparticles in the sol phase.

The mechanism of Pt formation from the ethoxide/hexachloroplatinic acid synthesis is proposed to involve a metathesis reaction [a chloride in H_2PtCl_6 is exchanged with an ethoxide group from $NaOC_2H_5$, resulting in an unstable $PtCl_5(OC_2H_5)^{2-}$ intermediate and NaCl], followed by a β-hydride elimination step, producing acetaldehyde and $PtCl_5H^{2-}$. Finally, a rapid reductive elimination step produces HCl and $PtCl_4^{2-}$. The process is repeated, reducing the Pt(II) species to Pt(0) nanoparticles.

Acknowledgment. We thank the University of Calgary and the Natural Sciences and Engineering Research Council of Canada (NSERC) for scholarship support of H.A.A. and overall financial support of this work. We also gratefully acknowledge the aid of the Alberta Synchrotron Institute (ASI) and Dr. Farideh Jahlilehvand for assistance in the interpretation of the XANES data. As well, we gratefully acknowledge the technical assistance of Qiao Wu and Jeremy Wulff of the University of Calgary in the collection of the NMR data and the helpful discussions with Dr. R. J. Puddephatt of the University of Western Ontario regarding the identity of the Zeise's salt analogue.

References and Notes

(1) Hill, J. M.; Dortright, R. D.; Dumesic, J. A. *Appl. Catal. A: Gen.* **1998**, *168*, 9.
(2) Sriramulu, S.; Jarvi, T. D.; Stuve, E. M. *Electrochim. Acta* **1998**, *44*, 1127.
(3) Liu, L.; Rameshkrishnan, V.; Liu, R.; Smotkin, E. S. *Electrochem. Solid State Lett.* **1998**, *1*, 123.
(4) Tamizhmani, G.; Dodelet, J. P.; Guay, D. *J. Electrochem. Soc.* **1996**, *143*, 18.
(5) Goodenough, J. B.; Hamnett, A.; Kennedy, B. J.; Manoharan, R.; Weeks, S. A. *Electrochim. Acta* **1990**, *35*, 199.
(6) Solla-Gullon, J.; Montiel, V.; Aldaz, A.; Clavilier, J. *J. Electroanal. Chem.* **2000**, *491*, 69.
(7) Mucalo, M. R.; Cooney, R. P. *J. Chem. Soc., Faraday Trans.* **1991**, *87*, 1221.
(8) Pron'kin, S. N.; Tsirlina, G. A.; Petrii, O. A.; Vassiliev, S. Y. *Electrochim. Acta* **2001**, *46*, 2343.
(9) Shan, J.; Pickup, P. G. *Electrochim. Acta* **2000**, *46*, 119.
(10) Park, K.-W.; Choi, J.-H.; Kwon, B.-K.; Lee, S.-A.; Sung, Y.-E. *J. Phys. Chem. B* **2002**, *106*, 1869.
(11) Zhao, S.-Y.; Chen, S.-H.; Wang, S.-Y.; Li, D.-G.; Ma, H.-Y. *Langmuir* **2002**, *18*, 3315.

(12) Martin, J. E.; Wilcoxon, J. P.; Odinek, J.; Provencio, P. *J. Phys. Chem. B* **2002**, *106*, 971.
(13) Wei, Z. D.; Zhang, S. T.; Tang, Z. Y.; Guo, H. T. *J. Appl. Electrochem.* **2000**, *30*, 723.
(14) Aika, K.; Ban, L. L.; Okura, I.; Namba, S.; Turkevich, J. *J. Res. Inst. Catal. Hokkaido Univ.* **1976**, *24*, 54.
(15) Furlong, D. N.; Launikonis, A.; Sasse, W. H. F. *J. Chem. Soc., Faraday Trans. 1* **1983**, *80*, 571.
(16) Brugger, P.-A.; Cuendet, P.; Gratzel, M. *J. Am. Chem. Soc.* **1981**, *103*, 2923.
(17) Antolini, E.; Cardelline, F.; Giacometti, E.; Squadrito, G. *J. Mater. Sci.* **2002**, *37*, 133.
(18) Birss, V. I.; Andreas, H. A.; Serebrennikova, I.; Elzanowska, H. J. *Electrochem. Solid State Lett.* **1999**, *2*, 326.
(19) Andreas, H.; Birss, V. I. *J. Electrochem. Soc.* **2002**, *149*, A1482.
(20) Andreas, H.; Birss, V. *J. Phys. Chem.*, in preparation.
(21) Andreas, H.; Birss, V. *Electrochim. Acta*, submitted for publication.
(22) Andreas, H.; Birss, V. *J. Electroanal. Chem.*, in preparation.
(23) Tsaprailis, H.; Birss, V. I. *Electrochem. Solid-State Lett.* **2004**, *7* (10), A348.
(24) McLeod, E.; Birss, V. *Electrochim. Acta*, submitted for publication.
(25) JADE; Release 5.0.12 ed.
(26) Carr, C.; Goggin, P. L.; Goodfellow, R. J. *Inorg. Chim. Acta* **1984**, *81*, L25.
(27) Cullity, B. C. *Elements of X-ray Diffraction*, 2nd ed.; Addison-Wesley Publishing Co. Inc.: Don Mills, Ontario, 1978; p 102.
(28) Puddephat, D. Personal communication.
(29) Seyferth, D. *Organometallics* **2001**, *20*, 2.
(30) Rosch, N.; Messmer, R. P.; Johnson, K. H. *J. Am. Chem. Soc.* **1974**, *96*, 3855.
(31) Olsson, A.; Kofod, P. *Inorg. Chem.* **1992**, *31*, 183.
(32) Cramer, R. *Inorg. Chem.* **1965**, *4*, 445.
(33) Atkins, P. *Physical Chemistry*; W. H. Freeman and Co.: New York, 1994; p 730.
(34) Greenwood, N. N.; Earnshaw, A. *Chemistry of the Elements*, 2nd ed.; Butterworth and Heinemann: Boston, 1997; p 1148.
(35) Anderson, J. S. *J. Chem. Soc.* **1934**, 971.
(36) Mayer, A. B. R.; Mark, J. E. *J. Polym. Sci., Part A: Polym. Chem.* **1997**, *35*, 3151.
(37) Pal, A.; Ghosh, K. G.; Esumi, K.; Pal, T. *Langmuir* **2004**, *20*, 575.
(38) Yonezawa, T.; Imamura, K.; Kimizuka, N. *Langmuir* **2001**, *17*, 4701.
(39) Bonnemann, H.; Braun, G.; Brijoux, W.; Brinkmann, R.; Schulze Tilling, A.; Seevogel, K.; Siepen, K. *J. Organomet. Chem.* **1996**, *520*, 143.